JOURNAL OF APPLIED ELECTROCHEMISTRY 26 (1996) 833–841

Electroconductive membrane 'Celec' for application in zinc/air alkaline batteries: An impedance study of oxygen reduction at the interface Pt/Celec

D. B. ZHOU, H. VANDER POORTEN

CTCN-FPMs, Polytechnic Faculty of Mons, Rue de l'Epargne, 56, B-7000 Mons, Belgium

Received 7 September 1995; revised 11 December 1995

Oxygen reduction was studied at a platinum electrode on a new ceramic membrane named 'Celec' in 6 M KOH with a view to application of this ceramic material in Zn/air batteries. Cyclic voltammetry and impedance measurements were carried out on the oxygen electrode to investigate the oxygen reduction mechanism in the presence of the 'Celec' ceramic. The impedance diagrams recorded at low and high overpotentials show different characteristics, which are well interpreted by the proposed mechanisms.

1. Introduction

Recently, we have developed a new ceramic material that can be used as ionic exchange membrane in the presence of aqueous electrolyte at room temperature.

The Celec ceramic material is of a zeolite structure. The basic components are layer silicates such as kaolinite, halloysite and montmorrillonite reinforced by silica and other minerals. The zeolite entities containing channels, cavities and windows permit transfer of water, gas and ions. As ionic conductor, the Celec material presents specific cationic conductivity. The oxide nature gives rise to electrocatalytic properties especially for oxygen reduction. The membrane thickness may vary considerably according to the proposed application and desired sizes.

The Celec membrane was at first used in the technology of ceramic electroformation. Further work has led to the application of this membrane in Zn/air batteries as the separate membrane and the porous air electrode support [1–3].

The present work concerns a fundamental study of oxygen reduction in the presence of this material in alkaline medium. The a.c. impedance technique, combined with potentiodynamic polarization measurements, is applied.

2. Experimental details

2.1. *Preparation of Celec membrane*

The Celec membrane was prepared from kaolin and potassium silicate. The raw material powder was calcined at 750 °C. The activated powder was added to an alkaline solution to form a slurry, which was cast in a mould. A polymerization process then yielded the desired solid shape.

The working electrode was a platinum wire of 0.4 mm diameter and 16 cm length, which was fixed on the down side of the Celec membrane during the casting process. A part of the platinum surface was in contact with the Celec membrane and another part exposed to gas, with the effective surface being about 1 cm^2.

2.2. *Apparatus*

Figure 1 shows the electrolytic cell for the electrochemical measurements. The Celec membrane was in the form of a cylindrical crucible, the base of which had a thickness of about 3 mm and served as the separating membrane for the gas and solution chamber.

The electrolyte was 6 M KOH prepared from high grade potassium hydroxide (Merck 5032) and distilled water. The counter electrode was a platinum plate with a surface area of 10 cm^2. The reference electrode was a Hg/HgO electrode connected to the cell via a Luggin capillary. Potential values reported in this paper are related to the Hg/HgO electrode. During measurements, oxygen was bubbled into the gas chamber passing through the surface of the platinum electrode. A small quantity of water was maintained in the bottom of the gas chamber to maintain moisture of the down side of the Celec membrane.

2.3. *Measuring techniques*

Two techniques were used in this study. Cyclic voltammetry measurements were performed using a potentiostat/galvanostat (EG&G PAR model 263) controlled with a computer program 'M270'. Impedance measurements were conducted at several d.c. potentials using an EG&G (model 5210) lock-in amplifier and a potentiostat/galvanostat. The a.c. frequency range was 100 kHz to 1 mHz. The a.c. impedance data were collected using an electrochemical program (M398).

0021-891X © 1996 Chapman & Hall

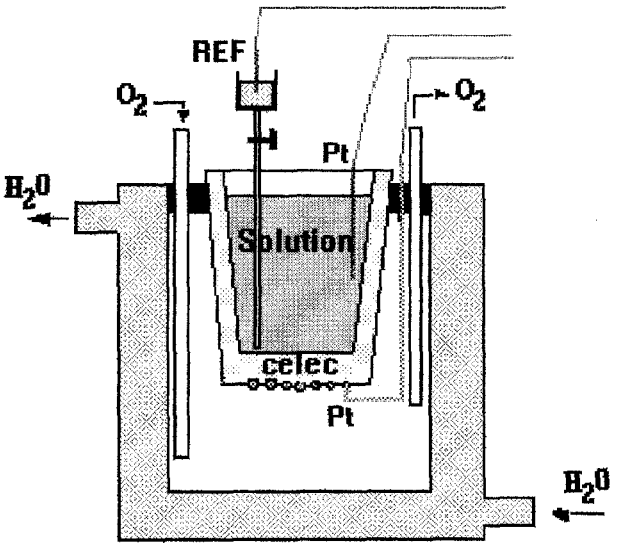

Fig. 1. Cell for the study of the oxygen reduction at the interface Pt/Celec.

3. Experimental results

3.1. *Cyclic voltammetry*

Cyclic voltammetry measurements were made in the 0.72 to −0.48 V and 0.18 to −0.98 V potential ranges. The scan rate was 100 mV s^{-1}. Figure 2 shows the voltammogram recorded between 0.72 and −0.48 V. It ranges from oxygen evolution to oxygen reduction. The diagram presents a similar behaviour to that obtained in aqueous electrolyte [4–7]. Platinum oxides were formed at potentials more positive than 0 V, giving an anodic plateau in the 0 V to 0.6 V range. The oxides were reduced at potentials more negative than 0 V producing a peak at about −0.3 V. This peak was partly due to oxygen reduction, which occurred after partial or total reduction of the platinum oxide.

The cathodic peak of the recorded curve is much smaller during the second cycle than during the first cycle. This is due to a smaller adsorbed oxygen concentration at the electrode surface during the second cycle.

The voltammogram recorded in the 0.18 to −0.98 V range (Fig. 3) appears quite different from that recorded in aqueous solution. Peaks corresponding to oxygen reduction or hydrogen desorption in the cathodic part are not found. On the return sweep, peaks due to hydrogen adsorption do not appear and the current is always negative. This behaviour, similar to that recorded on a gas diffusion electrode, shows that the Celec ceramic material can absorb much oxygen in its active structure.

3.2. *Impedance measurements*

The impedance measurements were conducted at several direct potentials: −0.1, −0.2, −0.3 and −0.4 V vs Hg/HgO. The corresponding Nyquist plots are shown in Fig. 4 to Fig. 7 respectively. At −0.1 V a small arc exists at high frequency range. A well defined capacitive semicircle appears at intermediate frequencies (1.58 kHz–10 mHz). At low frequencies (6.5–2.5 mHz), the plot approaches the real axis.

At −0.2 V, a small arc also exists at high frequencies. The capacitive semicircle is better defined and its diameter is decreased compared to that obtained at −0.1 V. At low frequencies, an inductive loop occurs. The impedance diagram recorded at −0.3 V is similar to that obtained at −0.2 V.

At −0.4 V the impedance diagram is quite different. The capacitive semicircle is a little depressed, possibly due to a Warburg impedance. At this potential, mass transfer processes cannot be ignored. In the lower frequency range (39.8–2.51 mHz), a complete inductive semicircle may be associated with an intermediate adsorption process. This is markedly different from the −0.1 V case.

4. Interpretation of the impedance characteristics

4.1. *Oxygen reduction (OR) mechanism at the interface Pt/Celec*

On a platinum electrode in alkaline solution, OR

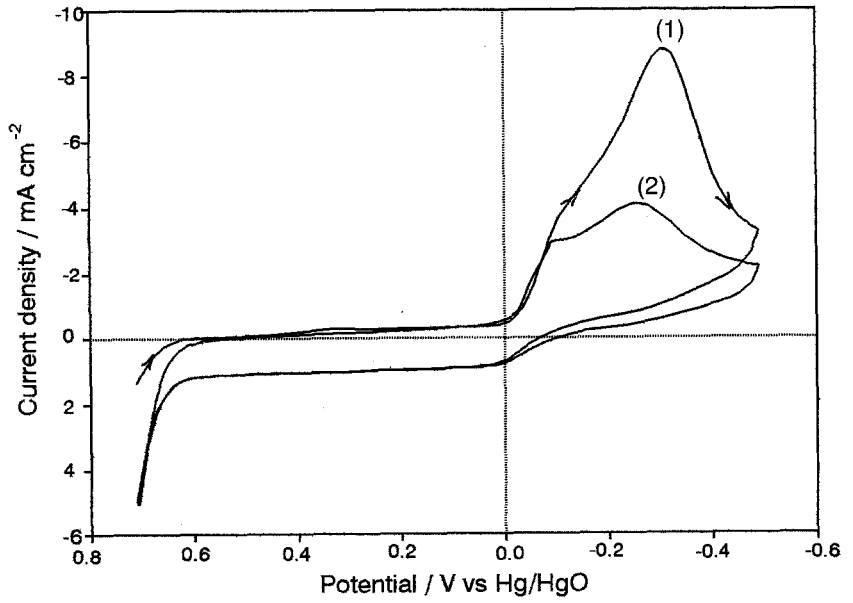

Fig. 2. Cyclic voltammogram at the interface Pt/Celec under O_2 at 20 °C. Potential range: +0.72 to −0.48 V; starting potential: +0.72 V, scan rate: 100 mV s^{-1}; (1) first cycle; (2) second cycle.

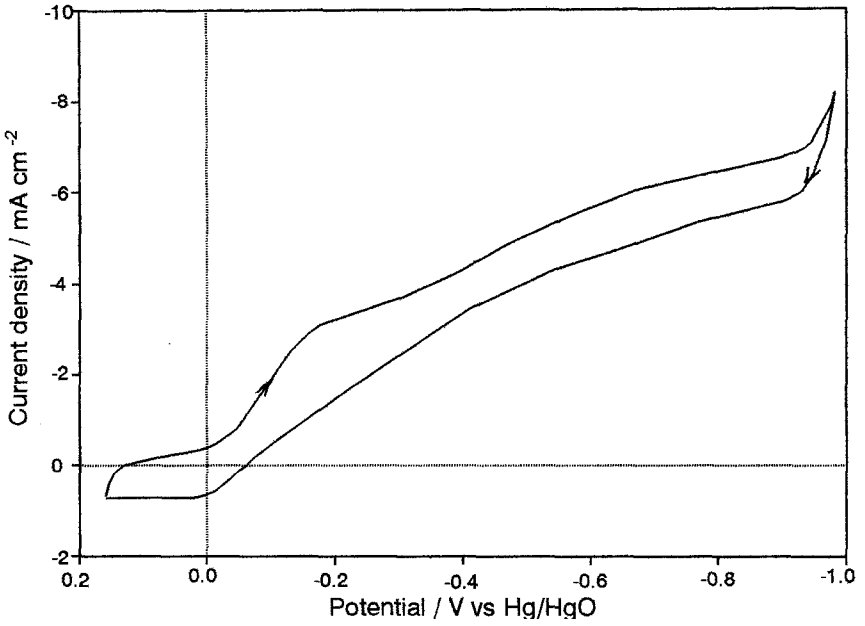

Fig. 3. Cyclic voltammogram at the interface Pt/Celec under O_2 at 20 °C. Potential range: 0.18 to −0.98 V; starting potential: +0.18 V; scan rate: 100 mV s^{-1}.

proceeds along a four electron or peroxide pathway depending on the electrode surface state. A clean surface favours the four electron path, while oxide or impurities coverage gradually favours the peroxide path.

The reduction of O_2 to OH^- or HO_2^- involves a charge transfer of several electrons. It is now generally accepted that OR mechanism involves an oxygen adsorption step followed by an electron transfer step which controls the rate of the overall reaction. Based on this consideration, various mechanisms have been proposed.

As reported elsewhere, and also shown in the present experimental work, the Tafel slope for OR at the platinum electrode is usually 60 mV dec^{-1} at low current density (c.d.) and 120 mV dec^{-1} at high c.d. This was attributed to two types of oxygen adsorption associated with two different electrode surface states: bridged and the end-on adsorption [8–13].

The mechanism of OR in alkaline electrolyte at low and high current densities might also be different. At low c.d., end-on adsorption would be favoured by the high coverage of the electrode surface with oxide or intermediate species. The bridged adsorption would be favoured at high c.d.

The cyclic voltammogram (Fig. 1) recorded at the interface Pt/Celec in the 0.72 to −0.48 V vs Hg/HgO potential range shows similar characteristics to those recorded in aqueous alkaline solution. This suggests that oxygen reduction in the presence of the Celec ceramic membrane occurs with a similar mechanism. Accordingly, the impedance characteristics recorded at the interface Pt/Celec in 6 M KOH are interpreted as follow.

At −0.1 V, the following OR mechanism is accepted [14]:

$$O_2 + e^- \xrightarrow{i} O_{2,ad}^- \qquad (1)$$

$$2O_{2,ad}^- + H_2O \xrightarrow{r} O_2 + HO_2^- + OH^- \qquad (2)$$

$$HO_2^- + H_2O \longrightarrow H_2O_2 + OH^- \qquad (3)$$

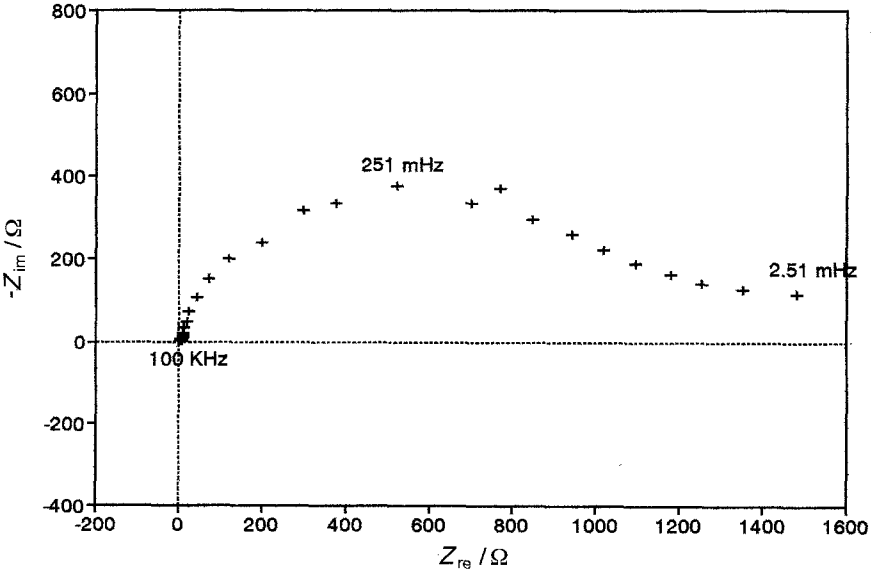

Fig. 4. Nyquist plot of impedance data obtained at interface Pt/Celec in 6 M KOH at 20 °C under O_2 atmosphere, $E_{dc} = -0.1$ V.

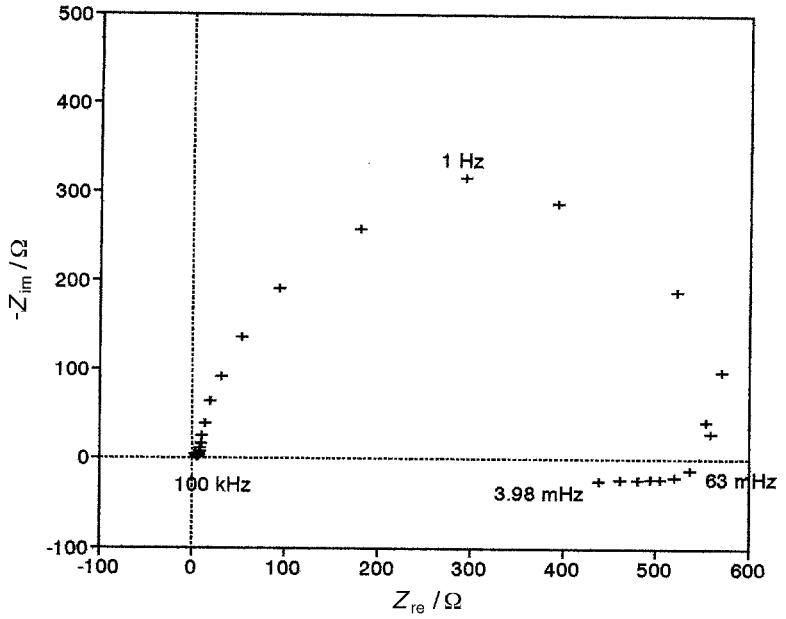

Fig. 5. Nyquist plot of impedance data obtained at interface Pt/Celec in 6 M KOH at 20 °C under O_2 atmosphere, $E_{dc} = -0.2$ V.

The charge transfer reaction (Reaction 1) is the rate-determining step. Reaction 2 is a catalytic reaction for which r represents the reaction rate. The formed HO_2^- may be thereafter reduced to OH^- at the electrode surface or reach the bulk of electrolyte. Reaction 3 corresponds to the equilibrium of HO_2^- and H_2O_2. The latter may exist in the electrolyte as final product.

The current density for Reaction 1 depends on the electrode potential (E), the coverage fraction of the electrode (θ) and the O_2 concentration at the Pt surface (C_o)

$$i = i(E, \theta, C_o) \tag{4}$$

The faradaic impedance of this mechanism, obtained from theoretical considerations, is [15]:

$$Z_F = R_{ct}\left[1 + \frac{\alpha}{j\omega + \tau}\right] - R_{ct}\frac{\partial i}{\partial C_O}\left[1 + \frac{\beta}{j\omega + \tau}\right]\frac{\overline{\Delta C_O}}{\overline{\Delta i}} \tag{5}$$

where R_{ct} is the charge transfer resistance,

$$\alpha = \frac{2\dfrac{\partial i}{\partial\theta}\dfrac{\partial r}{\partial E}}{\dfrac{\partial i}{\partial E}} - \frac{1}{F}\frac{\partial i}{\partial\theta} \tag{6}$$

$$\tau = 2\frac{\partial r}{\partial\theta} - \frac{2\dfrac{\partial i}{\partial\theta}\dfrac{\partial r}{\partial E}}{\dfrac{\partial i}{\partial E}} \tag{7}$$

$$\beta = \frac{2\dfrac{\partial i}{\partial\theta}\dfrac{\partial r}{\partial E}}{\dfrac{\partial i}{\partial E}} - \frac{2\dfrac{\partial r}{\partial C_o}\dfrac{\partial i}{\partial\theta}}{\dfrac{\partial i}{\partial C_o}} \tag{8}$$

The first term on the right side of Equation 5 represents the charge transfer resistance taking into account the effect of the intermediate $O_{2,ad}^-$ adsorption while the second term corresponds to the effect of oxygen concentration depending on the mass transport process.

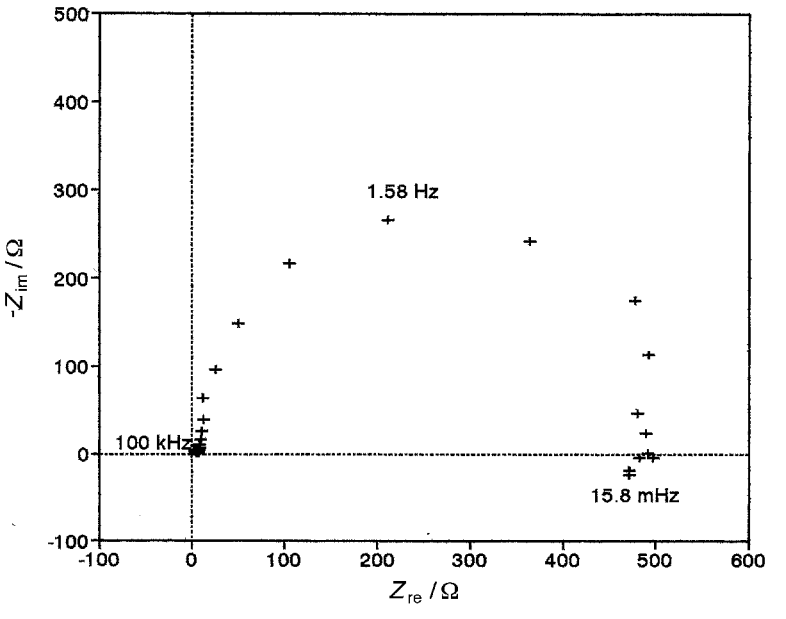

Fig. 6. Nyquist plot of impedance data obtained at interface Pt/Celec in 6 M KOH at 20 °C under O_2 atmosphere, $E_{dc} = -0.3$ V.

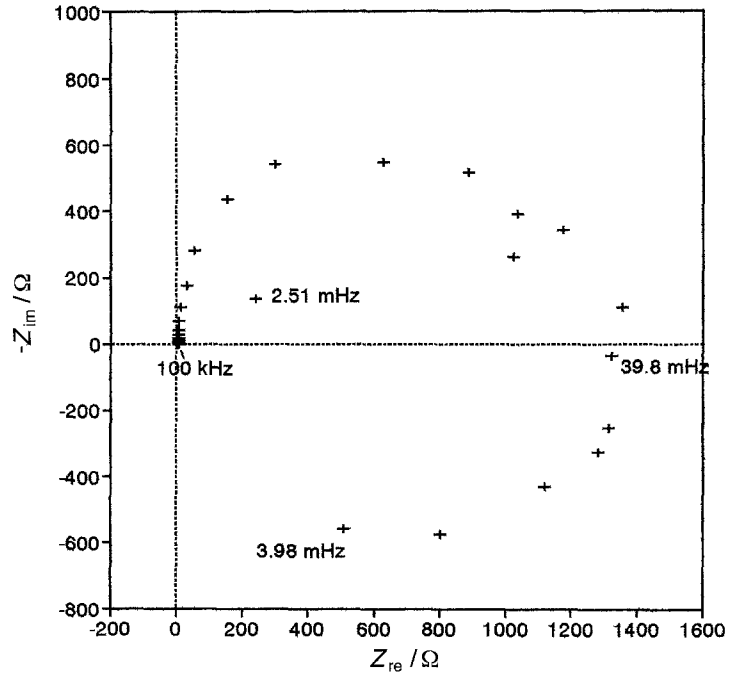

Fig. 7. Nyquist plot of impedance data obtained at interface Pt/Celec in 6 M KOH at 20 °C under O_2 atmosphere, $E_{dc} = -0.4$ V.

Assuming that the concentration effect is negligible, Equation 5 becomes

$$Z_F = R_{ct}\left[1 + \frac{\alpha}{j\omega + \tau}\right] \tag{9}$$

or

$$Z_F = R_{ct} + \frac{1}{j\omega\frac{1}{R_{ct}\alpha} + \frac{\tau}{R_{ct}\alpha}} \tag{10}$$

For Reaction 1 $\partial i/\partial\theta < 0$ and $\partial r/\partial\theta > 0$, so that the impedance expressed by Equation 10 corresponds to the electric circuit $R_{ct}(R_\theta C_\theta)$ represented in Fig. 8(a), with

$$C_\theta = \frac{1}{R_{ct}\alpha} \tag{11}$$

$$R_\theta = \frac{R_{ct}\alpha}{\tau} \tag{12}$$

The circuit description follows Boukamp's [16].

At −0.2 V and more negative potentials than −0.2 V, the OR mechanism is assumed to be [17]

$$O_{2,ad} + e^- \xrightarrow{i_1} O_{2,ad}^- \tag{13}$$

$$O_{2,ad}^- + H_2O \xrightarrow{r} HO_{2,ad} + OH^- \tag{14}$$

$$HO_{2,ad} + e^- \xrightarrow{i_2} HO_{2,ad}^- \tag{15}$$

where the current densities i_1 and i_2 depend on the electrode potential (E), the oxygen concentration at the platinum surface (C_o) and the coverage fractions (θ_1 and θ_2) of the electrode:

$$i_1 = i_1(E, C_o, \theta_1) \tag{16}$$

$$i_2 = i_2(E, \theta_1, \theta_2) \tag{17}$$

$$i = i_1 + i_2$$

Also, r is the reaction rate of Reaction 14

$$r = r(\theta_1, \theta_2) \tag{18}$$

In Equations 16–18 θ_1 and θ_2 correspond to $\theta_{O_{2,ad}^-}$ and $\theta_{HO_{2,ad}^-}$, respectively.

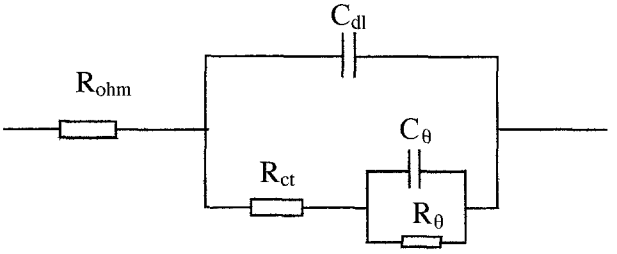

a) R(C[R(CR)])

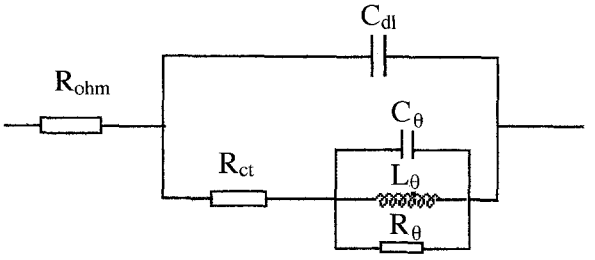

b) R(C[R(CRL)])

Fig. 8. Equivalent circuits adopted for oxygen reduction at the interface Pt/Celec in alkaline media at different potentials. The circuit description codes follow Boukamp's definition.

The corresponding faradaic impedance was similarly obtained [15]:

$$Z_F = \left(\frac{1}{R_{ct}} + \frac{j\omega \frac{1}{F}\left(\frac{\partial i_1}{\partial E}\frac{\partial i_1}{\partial \theta_1} - \frac{\partial i_2}{\partial E}\frac{\partial i_2}{\partial \theta_2}\right) + \frac{1}{F^2}\left(\frac{\partial i_1}{\partial E}\frac{\partial i_1}{\partial \theta_1}\frac{\partial i_2}{\partial \theta_2} + \frac{\partial i_2}{\partial E}\frac{\partial i_2}{\partial \theta_2}\frac{\partial i_1}{\partial \theta_1}\right) + \frac{1}{F}\left(\frac{\partial i_1}{\partial E}\frac{\partial r}{\partial \theta_1}\frac{\partial i_2}{\partial \theta_2} + \frac{\partial i_2}{\partial E}\frac{\partial r}{\partial \theta_2}\frac{\partial i_1}{\partial \theta_1}\right) - \frac{1}{F}\left(\frac{\partial i_1}{\partial E}\frac{\partial i_1}{\partial \theta_1}\frac{\partial r}{\partial \theta_2} + \frac{\partial i_2}{\partial E}\frac{\partial i_2}{\partial \theta_2}\frac{\partial r}{\partial \theta_1}\right)}{j\omega\left(\frac{1}{F}\frac{\partial i_2}{\partial \theta_2} - \frac{1}{F}\frac{\partial i_1}{\partial \theta_1} + \frac{\partial r}{\partial \theta_1} - \frac{\partial r}{\partial \theta_2}\right) + \frac{1}{F}\left(\frac{\partial r}{\partial \theta_1}\frac{\partial i_2}{\partial \theta_2} + \frac{\partial r}{\partial \theta_2}\frac{\partial i_1}{\partial \theta_1}\right) - \omega^2 - \frac{1}{F^2}\frac{\partial i_1}{\partial \theta_1}\frac{\partial i_2}{\partial \theta_2}} \right)^{-1}$$
$$\times \left\{ 1 - \left(\frac{\partial i}{\partial C_O} + \frac{j\omega \frac{1}{F}\frac{\partial i_1}{\partial C_O}\frac{\partial i_1}{\partial \theta_1} + \frac{1}{F^2}\frac{\partial i_1}{\partial C_O}\frac{\partial i_1}{\partial \theta_1}\frac{\partial i_2}{\partial \theta_2} + \frac{1}{F}\frac{\partial i_1}{\partial C_O}\left(\frac{\partial r}{\partial \theta_1}\frac{\partial i_2}{\partial \theta_2} - \frac{\partial i_1}{\partial \theta_1}\frac{\partial r}{\partial \theta_2}\right)}{j\omega\left(\frac{1}{F}\frac{\partial i_2}{\partial \theta_2} - \frac{1}{F}\frac{\partial i_1}{\partial \theta_1} + \frac{\partial r}{\partial \theta_1} - \frac{\partial r}{\partial \theta_2}\right) + \frac{1}{F}\left(\frac{\partial r}{\partial \theta_1}\frac{\partial i_2}{\partial \theta_2} + \frac{\partial r}{\partial \theta_2}\frac{\partial i_1}{\partial \theta_1}\right) - \omega^2 - \frac{1}{F^2}\frac{\partial i_1}{\partial \theta_1}\frac{\partial i_2}{\partial \theta_2}} \right) \frac{\overline{\Delta C_O}}{\overline{\Delta i}} \right\} \quad (19)$$

To simplify the expression (19), we introduce following parameters:

$$a_1 = -\frac{1}{F}\left(\frac{\partial i_1}{\partial E}\frac{\partial i_1}{\partial \theta_1} - \frac{\partial i_2}{\partial E}\frac{\partial i_2}{\partial \theta_2}\right)$$

$$a_2 = \frac{1}{F}\left(\frac{\partial i_1}{\partial E}\frac{\partial r}{\partial \theta_1}\frac{\partial i_2}{\partial \theta_2} + \frac{\partial i_2}{\partial E}\frac{\partial r}{\partial \theta_2}\frac{\partial i_1}{\partial \theta_1}\right)$$

$$a_3 = -\frac{1}{F^2}\left(\frac{\partial i_1}{\partial E}\frac{\partial i_1}{\partial \theta_1}\frac{\partial i_2}{\partial \theta_2} + \frac{\partial i_2}{\partial E}\frac{\partial i_2}{\partial \theta_2}\frac{\partial i_1}{\partial \theta_1}\right) - \frac{1}{F}\left(\frac{\partial i_1}{\partial E}\frac{\partial i_1}{\partial \theta_1}\frac{\partial r}{\partial \theta_2} + \frac{\partial i_2}{\partial E}\frac{\partial i_2}{\partial \theta_2}\frac{\partial r}{\partial \theta_1}\right)$$

$$b_1 = \left(\frac{1}{F}\frac{\partial i_2}{\partial \theta_2} - \frac{1}{F}\frac{\partial i_1}{\partial \theta_1} + \frac{\partial r}{\partial \theta_1} - \frac{\partial r}{\partial \theta_2}\right)$$

$$b_2 = \frac{1}{F}\left(\frac{\partial r}{\partial \theta_1}\frac{\partial i_2}{\partial \theta_2} + \frac{\partial r}{\partial \theta_2}\frac{\partial i_1}{\partial \theta_1}\right) - \frac{1}{F}\frac{\partial i_1}{\partial \theta_1}\frac{\partial i_2}{\partial \theta_2}$$

$$a_4 = -\frac{1}{F}\frac{\partial i_1}{\partial \theta_1}$$

$$a_5 = \frac{1}{F}\left(\frac{\partial r}{\partial \theta_1}\frac{\partial i_2}{\partial \theta_2} - \frac{\partial i_1}{\partial \theta_2}\frac{\partial r}{\partial \theta_2}\right)$$

$$a_6 = -\frac{1}{F^2}\frac{\partial i_1}{\partial \theta_1}\frac{\partial i_2}{\partial \theta_2}$$

For Reactions 13 to 15,

$$\frac{\partial i_1}{\partial E} > 0, \qquad \frac{\partial i_1}{\partial C_O} > 0, \qquad \frac{\partial i_1}{\partial \theta_1} < 0 \quad (20)$$

$$\frac{\partial r}{\partial \theta_1} > 0, \qquad \frac{\partial r}{\partial \theta_2} < 0 \quad (21)$$

$$\frac{\partial i_2}{\partial E} > 0, \qquad \frac{\partial i_2}{\partial \theta_2} > 0 \quad (22)$$

We have

$$a_i > 0 \qquad (i = 1 \text{ to } 6)$$

$$b_j > 0 \qquad (j = 1 \text{ to } 2)$$

Equation 19 therefore becomes

$$Z_F = \left(\frac{1}{R_{ct}} + \frac{-j\omega a_1 + a_2 - a_3}{j\omega b_1 + b_2 - \omega}\right)^{-1} \times \left\{ 1 - \left(1 + \frac{-j\omega a_4 - a_5 + a_6}{j\omega b_1 + b_2 - \omega}\right) \frac{\partial i}{\partial C_O}\frac{\overline{\Delta C_O}}{\overline{\Delta i}} \right\} \quad (23)$$

Ignoring concentration effects leads to

$$Z_F = \left(\frac{1}{R_{ct}} - \frac{a_1}{b_1} + \frac{a_1 b_2 + a_3 b_1 - a_2 b_1 - a_1 \omega^2}{j\omega b_1^2 + b_1 b_2 - b_1 \omega^2}\right)^{-1} \quad (24)$$

This corresponds exactly to the electric circuit $R(C[R(CLR)])$ represented in Fig. 8(b), with

$$R_\theta = \frac{b_2 R_{ct}}{b_i R_{ct} - b_2} \quad (25)$$

$$C_\theta = \frac{b_1 R_{ct} - b_2}{b_2 R_{ct}(b_1 - a_1 R_{ct})} \quad (26)$$

$$L_\theta = \frac{b_1 R_{ct} - b_2}{b_2^2 R_{ct}(b_1 - a_1 R_{ct})} \quad (27)$$

4.2. *Analysis of the experimental data*

Analysis of the experimental data was performed by fitting equivalent circuits [16]. The circuit shown in Fig. 8(a) was used at −0.1 V. Figure 9 shows experimental and fitted plots.

At high frequencies both plots reasonably agree but at low frequency, the proposed circuit does not correctly interpret the impedance behaviour. This means that the proposed mechanism generally describes the OR process but does not completely reveal the true situation.

At −0.2 V and −0.3 V, the circuit shown in Fig. 8(b) was applied. Figures 10 and 11 compare experimental and fitted diagrams. Both diagrams agree over the whole frequency range. This indicates that the proposed mechanism is reliable.

The experimental Nyquist diagram obtained at −0.4 V is in general agreement with the fitted diagram (Fig. 12). The large inductive semicircle at low frequencies is well reproduced. The match is nevertheless imperfect. At this potential, mass transfer effects might not be negligible. The corresponding Warburg or Nernst impedance element should therefore be added to the proposed circuit.

Impedance parameters obtained with the fitted equivalent circuits are given in Table 1 in which

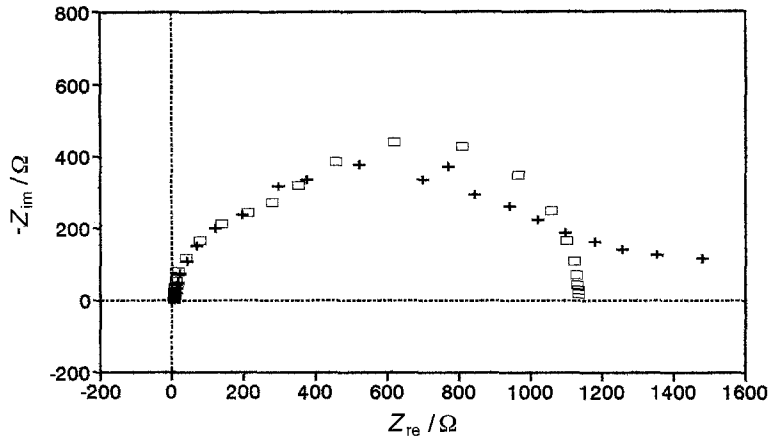

Fig. 9. Nyquist plot of impedance data fitted with equivalent circuit $R(C[R(CR)])$ (Fig. 8(a)) for oxygen reduction at −0.1 V. Key: (+) experimental data; (□) fit.

R_{ohm} is the ohmic resistance of the Celec membrane and aqueous electrolyte between the platinum and reference electrodes. The values obtained at different potentials are similar and range from 6.11 to 6.40 Ω.

The values of the double layer capacity C_{dl} measured at different potentials are also similar, (from 214 to 311 $\mu F\,cm^{-2}$). A double layer capacity of a platinum electrode plate around 20 $\mu F\,cm^{-2}$) was reported elsewhere. The value obtained at the Pt/Celec interface is more than 10 times bigger. This should not be attributed to the roughness of the electrode surface only. The nature of the Celec ceramic membrane is also important. An increase of the double layer capacity at increasing potential can be noticed.

With a single reaction, charge transfer resistance should decrease with increasing overpotential. Table 1 shows no significant dependence of R_{ct} on the direct current potential. This is because the OR mechanism involves several consecutive electron transfer reactions.

In Table 1, R_θ, C_θ and L are the parameters associated with the adsorption and desorption processes of intermediate species at the electrode surface. As these processes are very complicated, a quantitative analysis cannot be easily developed.

5. Conclusion

An ionic-conductive ceramic material named Celec has been developed for applications in alkaline air batteries. A fundamental study on the oxygen reduction at the interface Pt/Celec has been performed with cyclic voltammetry and a.c. impedance technique.

The voltammograms recorded at the Pt/Celec interface with a potential ranging from oxygen evolution to oxygen reduction (from +0.72 to −0.48 V vs Hg/HgO) showed characteristics similar to those recorded in aqueous alkaline media without any ceramics. The voltammogram recorded in more negative potential range (from +0.18 to −0.98 V vs Hg/HgO) presented a different behaviour from that recorded at the platinum electrode in aqueous solution.

The impedance plots obtained at low and high overpotentials presented different characteristics. The authors have elsewhere calculated two OR mechanisms for their impedance. The experimental results were well interpreted by the proposed mechanisms.

At low overpotential (−0.1 V vs Hg/HgO), the experimental results indicates that OR generally proceeds according to the mechanism represented by Reactions 1 to 3. At high overpotentials (from −0.2 to −0.4 V vs Hg/HgO), the mechanism shown by

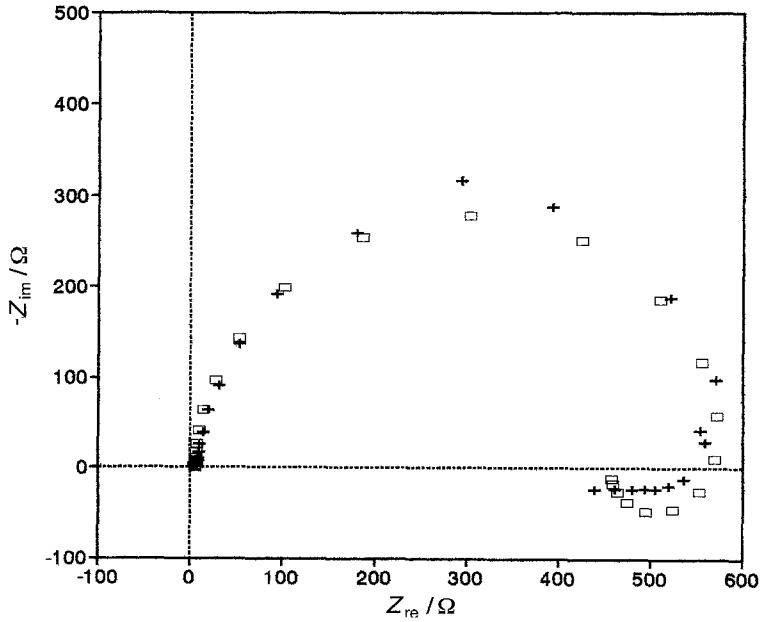

Fig. 10. Nyquist plot of impedance data fitted with equivalent circuit $R(C[R(CLR)])$ (Fig. 8(b)) for oxygen reduction at −0.2 V. Key: (+) experimental data; (□) fit.

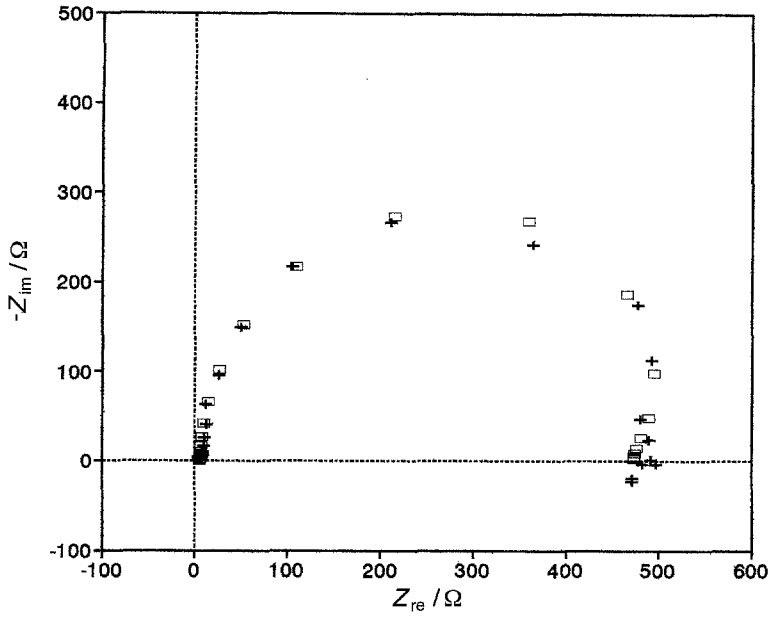

Fig. 11. Nyquist plot of impedance data fitted with equivalent circuit $R(C[R(CLR)])$ (Fig. 8(b)) for oxygen reduction at −0.2 V. Key: (+) experimental data; (□) fit.

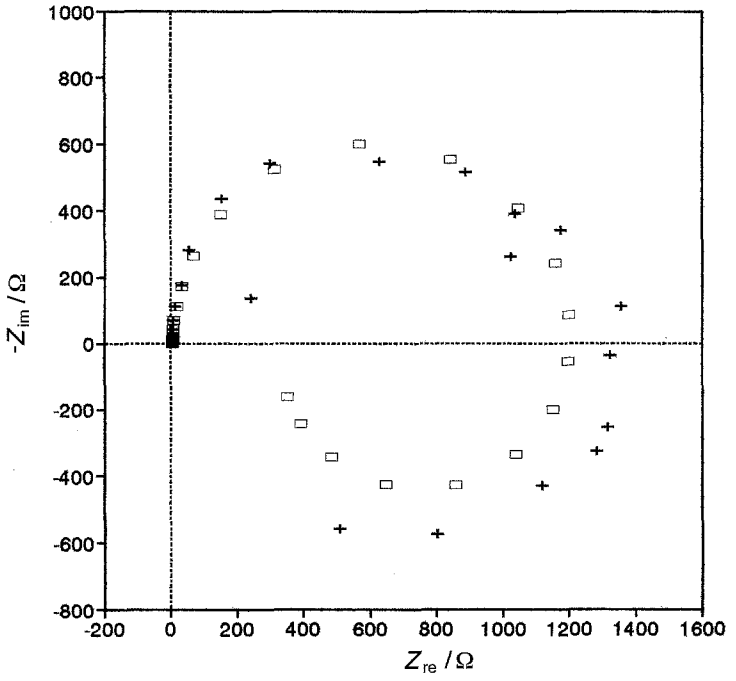

Fig. 12. Nyquist plot of impedance data fitted with equivalent circuit $R(C[R(CLR)])$ (Fig. 8(b)) for oxygen reduction at −0.4 V. Key: (+) experimental data; (□) fit.

Table 1. Impedance parameters for OR at the interface Pt/Celec in 6 M KOH at 20 °C

Potential /V *vs* Hg/HgO	*Equivalent circuit*	R_{ohm} /Ω	C_{dl} /μF	R_{ct} /Ω	R_θ /Ω	C_θ /μF	L /H
−0.1	$R(C[R(RC)])$	6.24	311	454	674	1510	
−0.2	$R(C[R(RCL)])$	6.12	242	450	125	637	504
−0.3	$R(C[R(RCL)])$	6.11	233	467	97	274	29.5
−0.4	$R(C[R(RCL)])$	6.40	214	311	88.9	22.7	1.0×10^4

Reactions 13 to 15 is in good agreement with experimental data.

References

[1] H. Vander Poorten, *US Patent SN0841 446* 22 Sept. 87 SIP, *SN921 158* 24 Nov. 87.

[2] D. B. Zhou, X. Y. Xiong and H. Vander Poorten, *Prog. Batteries & Battery Mater.* **13** (1994) 299–354.

[3] D. B. Zhou, X. Y. Xiong, D. G. Cao and H. Vander Poorten, 'Celec' ceramic membrane for use in alkaline batteries, 'Ninth international battery materials symposium', Cape Town, South Africa, March (1995), to be published in *Prog. Batteries & Battery Mater.*

[4] A. Kozawa, *J. Electronanal. Chem.* **8** (1964) 20.

[5] K. A. Striebel, F. R. Mclaron and E. J. Cairns, *J. Electrochem. Soc.* **137** (1990) 3351.

[6] A. Damjanovic, L-S. R. Yen and J. F. Wolf, *ibid.* **127** (1980) 1945.

[7] S. Park, S. Ho, S. Aruliah, M. F. Weber, C. A. Ward and R. D. Vender *ibid.* **133** (1986) 1641.

[8] A. Damjanovic, *Electrochim. Acta* **12** (1967) 615.

[9] *Idem, J. Electrochem. Soc.* **114** (1969) 1108.

[10] J. C. Huang, R. K. Sen and E. Yeager, *ibid* **126** (1979) 786.

[11] E. Yeager, *Electrochim. Acta* **29** (1984) 1527.

[12] D. B. Sepa, *ibid.* **25** (1980) 1491.

[13] K.-L. Hsueh, H. H. Chang, D.-T. Chin, *ibid.* **30** (1985) 1137.

[14] D. D. Macdonald, *in* 'Techniques for Characterisation of Electrodes and Electrochemical Processes' (edited by Ravi Varma and J. R. Selman), John Wiley & Sons, Inc. Pennington, New Jersey, 1991, chapter 11, p. 525.

[15] D. B. Zhou, PhD thesis, FPMs, Mons, Belgium (Feb 1996).

[16] B. Trémillon, 'Electrochimie Analytique et Réaction en solution', Tome 2, Masson, Paris (1993) p. 123.

[17] B. A. Boukamp, 'Equivalent Circuit', Twente University, PO Box 217, 7500 AE Enschede, The Netherlands (1989).